PHYSICAL REVIEW B **82**, 104410 (2010)

Charge transfer and tunable minority band gap at the Fermi energy of a quaternary $Co_2(Mn_xTi_{1-x})Ge$ Heusler alloy

P. Klaer,[1,*] T. Bos,[1] M. Kallmayer,[1] C. G. F. Blum,[2] T. Graf,[2] J. Barth,[2] B. Balke,[2] G. H. Fecher,[2] C. Felser,[2] and H. J. Elmers[1]

[1]*Institut für Physik, Johannes Gutenberg-Universität Mainz, D-55099 Mainz, Germany*

[2]*Institut für Anorganische Chemie und Analytische Chemie, Johannes Gutenberg-Universität Mainz, D-55099 Mainz, Germany*

(Received 14 July 2010; published 9 September 2010)

We investigate the distribution of element-specific magnetic moments and changes in the spin-resolved unoccupied density of states in a series of half-metallic $Co_2(Mn_xTi_{1-x})Ge$ Heusler alloys using x-ray magnetic circular dichroism. The Co and Mn magnetic moments are oriented parallel while a small Ti moment shows antiparallel to the mean magnetization. The element-specific magnetic moments remain almost independent on the composition. Therefore, a replacement of Ti by Mn results in an increase in magnetization. The increase in magnetization with increasing x follows the Slater-Pauling rule. The Fermi level decreases with respect to the minority band gap with increasing number of valence electrons. This counterintuitive behavior is explained qualitatively by a charge transfer model and quantitatively by *ab initio* band-structure calculations.

DOI: 10.1103/PhysRevB.82.104410 PACS number(s): 71.20.−b, 75.47.−m, 75.50.Cc, 78.70.Dm

I. INTRODUCTION

Ferromagnetic materials comprising a complete spin polarization at the Fermi level E_F have excited great scientific interest.[1,2] These materials, showing metallic conduction for one of the two spin channels and semiconducting or insulating behavior for the opposite spin channel, are called half-metallic ferromagnets (HMFs).[1] *Ab initio* theory has predicted HMF and a high Curie temperature for Co-based compounds comprising a band gap for minority electrons.[1,3–5] The main scientific and technological interest arises from HMF being very attractive materials for the fabrication of spintronic devices.[6–10] Recent experimental progress in the fabrication of tunneling magnetoresistance (TMR) devices provides indirect evidence for HMF in Heusler alloys because of the large TMR values[7,8,10–13] observed for magnetic tunneling junctions using Heusler electrodes.

In order to tune the Fermi energy of a Heusler alloy (common chemical formula X_2YZ) with respect to the minority band gap, a band structure tailoring through substitution of the transition metal on the Y site or the main group element on the Z site in quaternary compounds has been proposed.[5,9,14–16] Shan *et al.*[17] presented a tunneling spectroscopy study that supports this idea of band structure tailoring for $Co_2Fe(Al_{0.3}Si_{0.7})$. Sakuraba *et al.*[18] confirmed this idea by an investigation of a $Co_2Fe(Al_{1-x}Si_x)$ series. A shift of the band gap for $Co_2(Fe_xMn_{1-x})Si$ has also been tested by photoemission spectroscopy without spin resolution.[19,20] Recently, an analysis scheme of x-ray magnetic circular dichroism (XMCD) data was presented offering an experimental access to the unoccupied part of the Co-related density of states (DOS),[21,22] that determines the edges of the minority band gap.[3,23,24] For epitaxial $Co_2(Fe_xMn_{1-x})Si$ and $Co_2Fe(Al_{1-x}Si_x)$ film series grown on MgO(100) a systematic variation in the position of E_F with the composition was found[21] and quantitatively compared to theory. A bulk sample series of $Co_2Mn(Ga_{1-x}Ge_x)$ also showed a systematic shift of the Fermi level with composition[22] and an increased spin polarization for $x=0.75$.[25]

In all the examples mentioned above the shift of the Fermi level follows a rigid-band model. Assuming a rigid-band structure independent on composition, additional electrons stemming from an increasing number of valence electrons fill up majority states, thus increasing the magnetization and also the Fermi level with respect to the minority band gap. This behavior is equivalent to the generalized Slater-Pauling rule confirmed by *ab initio* calculations.[26,27] In this paper we report on a sample series of $Co_2(Mn_xTi_{1-x})Ge$ showing the opposite behavior, i.e., the Fermi level decreases with increasing valence-electron number while the magnetization still increases. As an explanation for this behavior a qualitative charge transfer model is depicted. The experimental results are compared to *ab initio* band-structure calculations.

II. EXPERIMENTAL

The polycrystalline samples were prepared by arc-melting of stoichiometric quantities of the constituents in an argon atmosphere (10^{-4} mbar). Care was taken to avoid oxygen contamination. This was established by evaporation of Ti inside of the vacuum chamber before melting the compound as well as additional purification of the process gas. The melting procedure was repeated three times to get a homogeneous material. After melting, the polycrystalline ingots were annealed in an evacuated quartz tube at 1073 K for 8 days. For powder investigations, a part of the sample was crushed by hand using a mortar.

The structure was investigated by x-ray diffraction using excitation by Mo $K\alpha$ (Bruker, D8) radiation of powder samples. All samples exhibit the Heusler $L2_1$ structure with a small B2 type disorder contribution. The magnetic properties were investigated by a superconducting quantum interference device (SQUID, Quantum Design MPMS-XL-5) using nearly punctual sample pieces of approximately 10–20 mg. Rods with dimensions $1\times1\times10$ mm^3 were cut from the ingots for spectroscopic investigations of the bulk samples.

X-ray absorption spectroscopy (XAS) experiments were performed at the UE56/1-SGM beamline at the German syn-

TABLE I. Relative atom concentration given as percentages of the samples from the $Co_2(Mn_xTi_{1-x})Ge$ series according to an EDX analysis.

x	Co	Mn	Ti	Ge
0.0	49.5	0.0	23.2	27.3
0.2	49.8	4.8	20.7	25.1
0.4	49.2	10.2	14.9	25.7
0.5	49.9	12.5	12.4	25.2
0.6	49.4	15.0	10.1	25.5
1.0	49.2	25.3	0.0	25.5

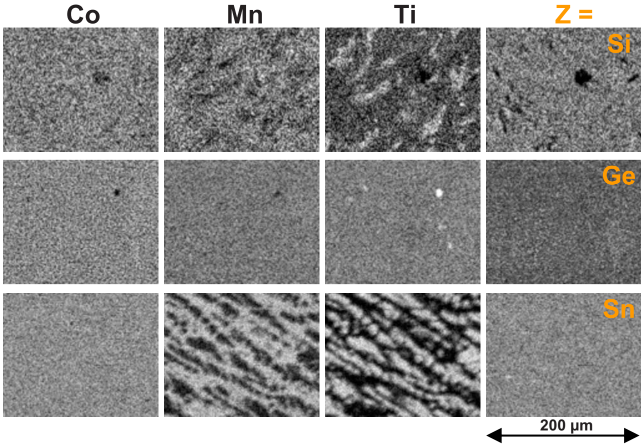

FIG. 1. (Color online) Element-specific EDX mappings for the series $Co_2(Mn_{0.6}Ti_{0.4})Si$ (first line), $Co_2(Mn_{0.6}Ti_{0.4})Ge$ (second line), and $Co_2(Mn_{0.6}Ti_{0.4})Sn$ (third line). The columns show the elements Co, Mn, and Ti, and Z=Si, Ge, and Sn, respectively. The brightness represents qualitatively the element concentration.

chrotron light source BESSY II. The samples were fractured *in situ* in UHV ($p = 1 \times 10^{-9}$ Torr) directly before the measurement. An Au mesh monitored the incident photon flux. The total electron yield served as a measure for the x-ray absorption signal. The sample was shielded by a conducting tube in order to collect all electrons. An external magnetic field of 1.22 T was applied along the direction of the incident x-ray beam, i.e., approximately perpendicular to the sample surface, and switched after each data point to determine the XMCD signal while the polarization was kept constant. The energy resolution of the x-ray monochromator was set to approximately 0.4 eV at 800 eV photon energy. An increase in the resolution to 0.1 eV at 800 eV for selected samples revealed only marginal changes in the observed spectra. This confirmed that the spectral shape is dominated by the intrinsic lifetime broadening of x-ray absorption.

After these measurements a scanning electron microscope (SEM, Jeol JSM-6400) equipped with an energy-dispersive x-ray spectroscopy (EDX) detection system was used to check the homogeneity and stoichiometry of the samples. An acceleration voltage of 20 kV and an inspection angle of 35° was set up. The quantitative data was corrected by the ZAF method which relies on atomic number (Z), absorption (A), and fluorescence (F) effects. One should note that the accuracy of the determination of the relative atomic concentration is on the order of ±2 at. %.

III. PHASE HOMOGENEITY

From the EDX analysis of the sample surfaces we obtain the relative atomic compositions according to Table I. Within error limits the average composition reproduces the desired composition for the $Co_2(Mn_xTi_{1-x})Ge$ series. Element-specific EDX mappings (Fig. 1) reveal the spatial distribution of the composition for the $Co_2(Mn_xTi_{1-x})Ge$ series. For comparison results for $Co_2(Mn_{0.6}Ti_{0.4})Si$ from Ref. 22 and $Co_2(Mn_{0.6}Ti_{0.4})Sn$ from Ref. 28 are included. The $Co_2(Mn_xTi_{1-x})Ge$ samples have a homogeneous composition, in contrast to $Co_2(Mn_xTi_{1-x})Si$ and to $Co_2(Mn_xTi_{1-x})Sn$ which show a decomposition into a Co_2MnZ-enriched and Co_2TiZ-enriched (with Z=Si and Sn, respectively) phase.

The different behavior of the three $Co_2(Mn_{1-x}Ti_x)Z$ series with Z=Si, Ge, and Sn might be explained by the different size of the atoms in the Z position. While Si is smaller and Sn larger compared to Co, Mn and Ti, Ge has nearly the same size. From the hard sphere model one easily imagines that the internal stress for a mixed compound of unequally sized atoms can be reduced by decomposition. This model is supported by the observation of a smaller lattice constant variation with x for Z=Ge compared to Z=Si and Sn shown in Fig. 2 (values taken from Ref. 29).

A reason for the particular shape of decomposed phases are the higher melting points for the Co_2TiZ (Z=Si and Sn) phase than for the Co_2MnZ (Z=Si and Sn) phase. This leads to an initial crystallization of the Co_2TiZ-enriched phase during cooling, revealing the rounded Co_2TiZ-rich areas in a matrix consisting of the Co_2MnZ-enriched Heusler phase.

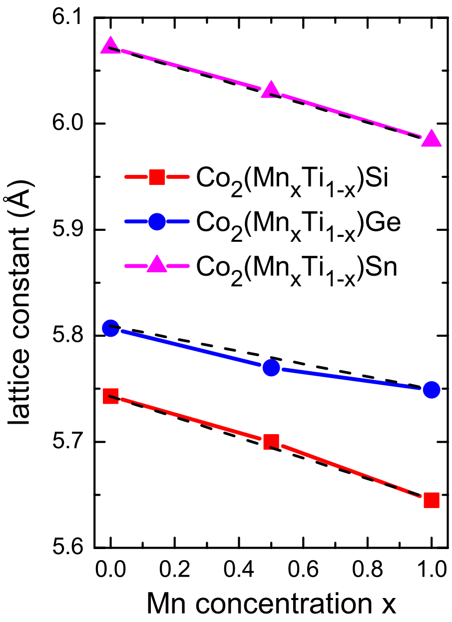

FIG. 2. (Color online) Lattice constant variation depending on the Mn concentration.

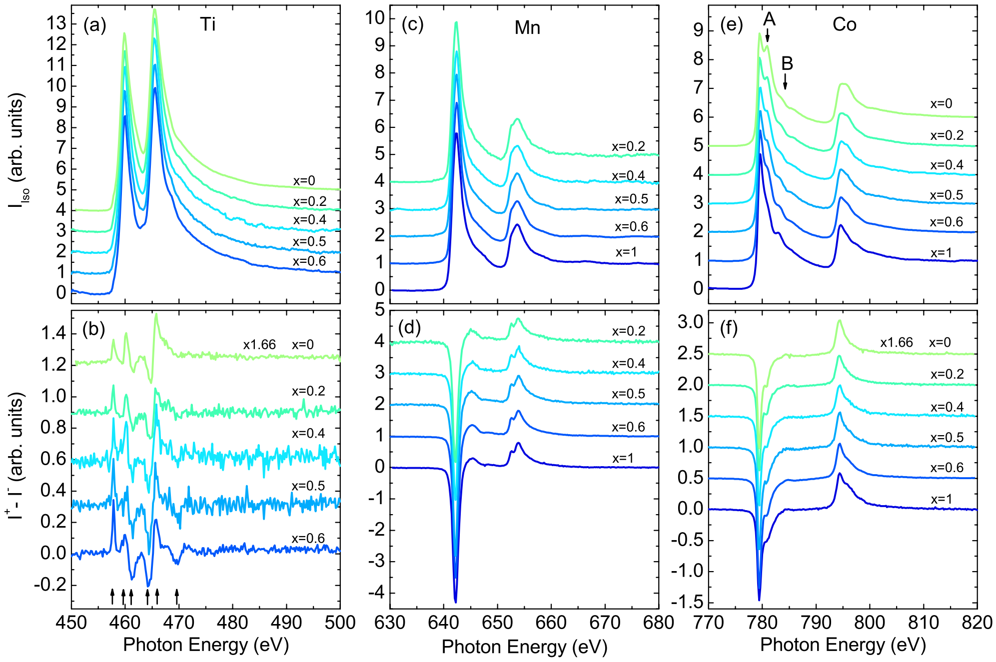

FIG. 3. (Color online) [(a), (c), and (e)] X-ray absorption spectra for $Co_2(Mn_xTi_{1-x})Ge$ measured at the $L_{3,2}$ edge averaged from total electron yield intensities I^+ and I^- for magnetization direction parallel and antiparallel to the x-ray polarization. [(b), (d), and (f)] Corresponding XMCD spectra $I^+ - I^-$.

IV. X-RAY ABSORPTION SPECTROSCOPY AND MAGNETIC MOMENTS

XAS/XMCD results are shown in Fig. 3 for the $Co_2(Mn_xTi_{1-x})Ge$ series measured at the Ti $L_{3,2}$, Mn $L_{3,2}$, and Co $L_{3,2}$ edges. All measurements were performed at 110 K except for $x=0$ which was done at 300 K. For consideration of the thermal magnetization decrease, we multiplied the room-temperature XMCD signal of the sample with $x=0$ by a factor of 1.66. The Co XAS spectra in Fig. 3(e) reveal the largest change with composition. Similar changes occur at the L_3 edge and L_2 edge. Replacing Ti by Mn causes a vanishing of the second maximum A (~1 eV above L_3 maximum) and an arising satellite peak B (~4 eV above). Peak A represents a dominant Co-Ti *d*-band hybridization state. The satellite peak B corresponds to a Co-Mn *sd*-band hybridization state and was described as characteristic for highly ordered Heusler compounds.[30] In the quaternary Heusler alloy Mn has also some effects on the Ti states and the corresponding XMCD spectra. A systematic change in the peak height and an additional feature at 470 eV occurs in the Ti XMCD spectra [marked in Fig. 3(b)].

From the element-specific XMCD spectra we derived the magnetic spin moment μ_{spin} and the magnetic orbital moment μ_{orb} shown in Table II using the sum-rule analysis assuming numbers of *d* holes $N_h(Co)=2.5$, $N_h(Mn)=4.5$, and $N_h(Ti)=8$ and for Mn a *jj*-mixing correction factor $i=1.5$ as described in Ref. 31. Similar experimental moments were reported[32] for Co_2MnGe ($x=1$) with slightly larger Co and smaller Mn orbital moments. Theoretical results for Co_2MnGe (Table II) coincide with previously reported data.[33] $Co_2(Mn_xTi_{1-x})Ge$ is a ferrimagnet due to the antiparallel magnetic moments of Ti and Co/Mn. The increase in the Mn content leads to a strong increase in the negative Ti magnetic moment. The Co spin moment slightly increases with *x* and the Mn spin moment remains almost constant.

Figure 4 shows the XMCD corresponding total magnetic moments and the measured SQUID values at 110 K. The experimental results are not far away from the Slater-Pauling curve and the *ab initio* local-density approximation plus *U* (LDA+*U*) calculations (only spin magnetic moments). Re-

TABLE II. Element-specific magnetic spin moments μ_{spin} and orbital moments μ_{orb} per atom for the $Co_2(Mn_xTi_{1-x})Ge$ series as calculated from the sum rules. Magnetic spin moments μ_{spin}(LDA) from the LDA+*U* calculations are given for comparison.

x	μ	Co	Mn	Ti
0.0	μ_{spin}	0.69 ± 0.02		-0.03 ± 0.05
	μ_{spin}(LDA)	1.05		−0.05
	μ_{orb}	0.06 ± 0.01		
0.2	μ_{spin}	0.62 ± 0.02	3.18 ± 0.10	-0.04 ± 0.05
	μ_{orb}	0.05 ± 0.01	0.03 ± 0.05	
0.4	μ_{spin}	0.68 ± 0.02	3.21 ± 0.10	-0.04 ± 0.05
	μ_{orb}	0.05 ± 0.01	0.04 ± 0.05	
0.5	μ_{spin}	0.79 ± 0.02	3.84 ± 0.10	-0.05 ± 0.05
	μ_{spin}(LDA)	1.01	3.19	−0.1
	μ_{orb}	0.08 ± 0.01	0.11 ± 0.05	
0.6	μ_{spin}	0.81 ± 0.02	3.64 ± 0.10	-0.06 ± 0.05
	μ_{orb}	0.08 ± 0.01	0.04 ± 0.05	
1.0	μ_{spin}	0.93 ± 0.02	3.25 ± 0.10	
	μ_{spin}(LDA)	1.02	3.05	
	μ_{orb}	0.00 ± 0.01	0.24 ± 0.05	

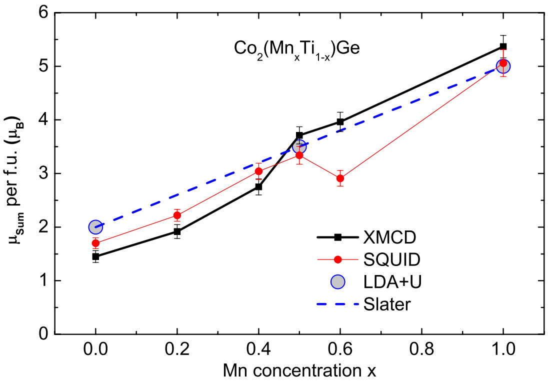

FIG. 4. (Color online) Total magnetic moments for Co$_2$(Mn$_x$Ti$_{1-x}$)Ge measured at 110 K with SQUID and XMCD as a function of the Mn concentration. The dashed line indicates the Slater-Pauling rule.

markable is the Slater-Pauling curve crossing of the total magnetic moment at $x=0.5$ derived from XMCD. Crystalline disorder has a direct effect on the magnetic moment. B2 disorder in the samples is hardly avoidable and leads to an increased magnetic moment for $x>0.5$ (in the ferromagnetic dominated case) and a decreased magnetic moment for $x<0.5$ (ferrimagnetic dominated case).

V. SPIN-RESOLVED UNOCCUPIED DENSITY OF STATES

Self-consistent electronic-structure calculations were carried out using the full-potential linearized augmented plane-wave method as implemented in WIEN2K.[34] Further details for the *ab initio* LDA+U calculations can be found in Ref. 24. As previously discussed[3] the theoretical results for Co$_2$(Mn$_x$Ti$_{1-x}$)Ge ($x=0,0.5,1$) in Fig. 5 show that the boundaries of the minority band gap at E_F are dominated by the Co states. A minority band gap occurs for the complete Co$_2$(Mn$_x$Ti$_{1-x}$)Ge series indicating half-metallic behavior. The Fermi energy is shifted from a position close to the conduction-band edge for Co$_2$TiGe to a position near the valence-band edge for Co$_2$MnGe. Hence, an experimental test of the calculated band gap can be restricted to the Co related DOS.

The experimental spin-resolved unoccupied Co partial DOS (PDOS) is shown in Fig. 6 derived from the Co L_3-edge absorption data. For the calculation we used the spin-resolved unoccupied PDOS function (Fermi function f_F) following from the XAS spectra I^+ and I^-,

$$D^{\uparrow(\downarrow)}(1-f_F) \propto I_{iso} - s + (-)\frac{1}{P_j}\frac{I^+ - I^-}{2}, \tag{1}$$

where I_{iso} denotes the isotropic absorption coefficient $(I^+ + I^-)/2$, s is the step function, and P_j is the spin polarization of the excited photoelectrons, i.e., $P_{L3}=0.25$ and $P_{L2}=-0.5$. An electron correlation effect causes a shift of the majority PDOS of $\Delta E_c=0.5$ eV with respect to the minority states as explained in Refs. 21 and 22. The position of the Fermi level was derived from the initial increase in the majority states considering the energy shift of ΔE_c.

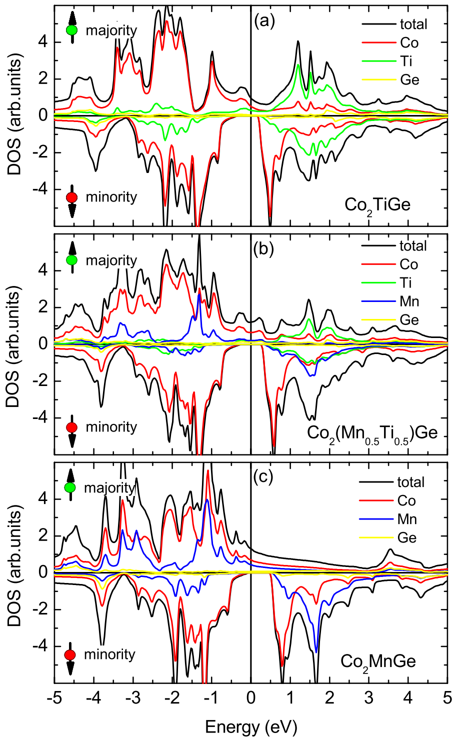

FIG. 5. (Color online) Spin-resolved DOS for Co$_2$(Mn$_x$Ti$_{1-x}$)Ge ($x=0,0.5,1$) as indicated in the figure using *ab initio* LDA+U calculations.

Due to the lifetime broadening of the XAS spectra we have deconvoluted the experimental spectra with a Lorentzian function with a width of $\Gamma=0.35$ eV. Note, that the Co minority PDOS is close to zero in a finite energy interval around E_F. The observation of a vanishing PDOS for $E<E_F$ is a consequence of a near coincidence of the Lorentzian function and the experimental data. Thus, the experimental data support the theoretical prediction of half-metal behavior particular for Co$_2$MnGe. In comparison with the LDA+U calculations we can find a nice coincidence [see Figs. 6(a), 6(c), and 6(f)]. Only Co$_2$MnGe shows a deviation in the majority states which has not been understood yet. Co-Ti d-hybridization states are well reproduced in the minority states (1.8 eV above E_F). Even though, from the experimental results one can assume that the Co-Ti hybridization state should be more pronounced in the calculations.

Replacing Ti by Mn reduces the difference $E_{v,max}-E_F$ between the prominent maximum $E_{v,max}$ in the minority PDOS and E_F as indicated in Fig. 6(a). Results for $E_{v,max}-E_F$ are summarized in Fig. 7 and compared to *ab initio* calculations. The theoretical results show a good agreement with the experimental results. The linear increase in $E_{v,max}-E_F$ with increasing valence electron number N_v is quantitatively reproduced. This indicates that the predict half metallicity for this series exist in the samples. Figure 7 also shows the results for isoelectronic Co$_2$(Mn$_x$Ti$_{1-x}$)Ge and Co$_2$Mn(Ga$_{1-x}$Ge$_x$) series from Ref. 22 for comparison. Instead of an increasing value of $E_{v,max}-E_F$, Co$_2$(Mn$_x$Ti$_{1-x}$)Si shows only one step from $x=0.8$ to $x=1$. This can be explained by the phase inhomogeneity discussed before. Co$_2$TiSi impurities in the quaternary Co$_2$(Mn$_x$Ti$_{1-x}$)Si compound dominate the energetic position

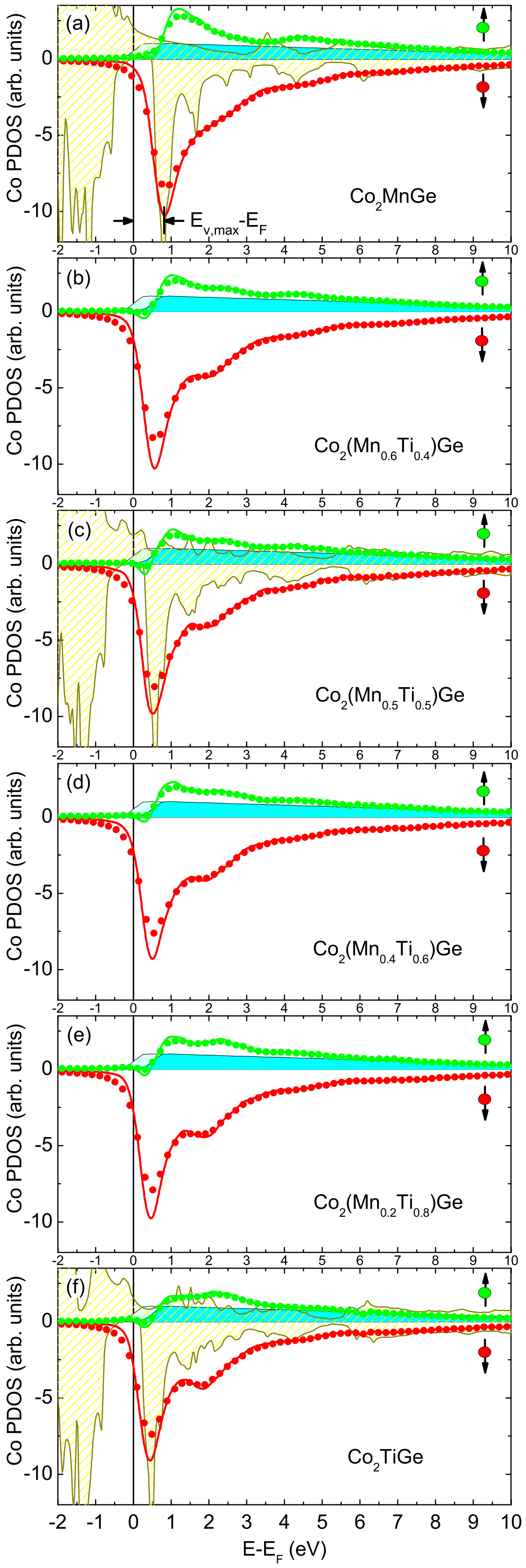

FIG. 6. (Color online) Spin-resolved PDOS calculated from the XAS/XMCD data (dots) measured at the L_3 edge for Co$_2$(Mn$_x$Ti$_{1-x}$)Ge samples as indicated in the figure. Full lines show the deconvoluted data. Full filled areas indicate the function used for approximation of the itinerant band as measured (blue) and shifted by ΔE_c (light blue). Data from theoretical *ab initio* calculations are indicated by a yellow patterned area in (a), (c), and (f).

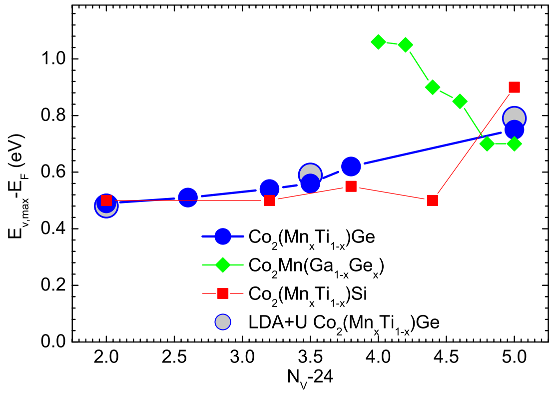

FIG. 7. (Color online) Separation of the minority PDOS maximum and the Fermi energy $E_{v,max}-E_F$ for the indicated Heusler alloys (full symbols). N_v indicates the number of valence electrons per formula unit.

of $E_{v,max}-E_F$. A completely different behavior is observed for Co$_2$Mn(Ga$_{1-x}$Ge$_x$). In this case we observe a linear decrease in $E_{v,max}-E_F$ with increasing N_v. The decrease in $E_{v,max}-E_F$ is a consequence of filling the majority Co states with electrons. This shifts the Fermi energy to the right side of the band gap as expected from the rigid-band model. At first glance a similar behavior was expected for Co$_2$(Mn$_x$Ti$_{1-x}$)Ge, too. However, obviously the rigid-band model is too simple, as it does not explain the experimental result. The result for Co$_2$(Mn$_x$Ti$_{1-x}$)Ge can instead be explained by the charge transfer sketched in Fig. 8. Ti has a very small electronegativity compared to Co. This causes charge transfer from Ti to Co in Co-Ti *d*-hybridization states (t_{2g} states) as displayed in (a) for Co$_2$TiGe. If Ti atoms are replaced by Mn (b) the electrons are redistributed. Mn has an electronegativity between Ti and Co. The electron transfer from Mn to Co is less pronounced. Moreover, electrons are shifted from Ti to Mn instead to the Co sites. The Mn-Ti charge transfer causes an additional loss of occupied majority Ti states at E_F and an increasing of the negative magnetic Ti moment (see also Table II). The redistribution increases with increasing number of replaced Ti atoms. Thus the increasing electronegativity Ti-Mn-Co leads to an emptying of majority Co *d* states near E_F. Accordingly, E_F shifts to the left side of the minority band gap. Without Ti (c) we have

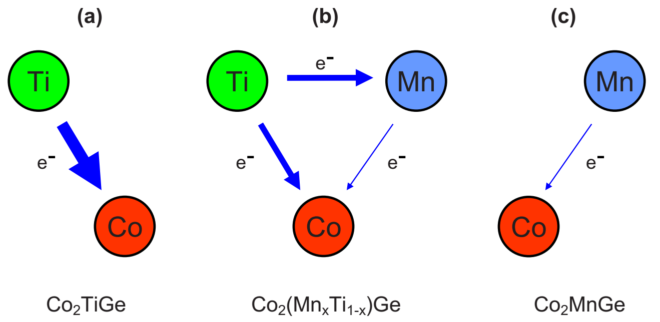

FIG. 8. (Color online) Charge transfer sketch for the (a) Co$_2$TiGe, (b) Co$_2$(Mn$_x$Ti$_{1-x}$)Ge, and (c) Co$_2$MnGe compound. The arrows represent the direction and the amount of the electron transfer between the atoms.

only a small Mn-Co charge transfer. A similar electron transfer scheme was already considered for binary bulk alloys by Friedel.[35]

VI. SUMMARY

In our work we present magnetic and electronic properties of a quaternary $Co_2(Mn_xTi_{1-x})Ge$ Heusler alloy series. The whole series is predicted to be ferromagnetic (ferrimagnetic) half metallic. The homogeneity of the phase was proved by element-specific EDX mapping. The results show a homogeneous phase in contrast to $Co_2(Mn_xTi_{1-x})Si$ and $Co_2(Mn_xTi_{1-x})Sn$. Element-specific magnetic moments and the spin-resolved unoccupied density of states were investigated using XMCD. The small Ti magnetic spin moment oriented antiparallel to the spin moments of Co and Mn confirm the theoretical *ab initio* LDA+U calculations. From XAS/XMCD we have derived the spin-resolved unoccupied Co density of states. The experimental results are in close agreement with *ab initio* calculations. We find an increasing value of $E_{v,max}-E_F$ with increasing Mn content for $Co_2(Mn_xTi_{1-x})Ge$, which cannot be explained by the rigid-band model as in the case for $Co_2Mn(Ga_{1-x}Ge_x)$. This unexpected behavior can only be accounted for by a charge transfer from Ti to Co and Mn due to the small electronegativity of Ti in combination with the half metallicity. Therefore, the $Co_2(Mn_xTi_{1-x})Ge$ quaternary Heusler alloy allows a tailoring of the Fermi energy position within the minority DOS band gap.

From this suggested charge transfer model one may conclude that $Co_2(Fe_xTi_{1-x})Z$ and $Co_2(Cr_xTi_{1-x})Z$ (Z=Si and Ge) series behave in a similar way. Calculations for the parent compounds Co_2FeZ (Z=Si and Ge) (Ref. 36) and Co_2CrSi (Ref. 37) as well as the experimental result for Co_2FeSi (Ref. 21) support this idea.

ACKNOWLEDGMENTS

The authors are thankful for financial support from the DFG (Grant No. FOR 559) and BMBF (Grant No. ES3XBA/5), and S. Cramm for support at BESSY.

---

*klaer@uni-mainz.de

[1] R. A. de Groot, F. M. Mueller, P. G. van Engen, and K. H. J. Buschow, Phys. Rev. Lett. **50**, 2024 (1983).

[2] J.-H. Park, E. Vescovo, H.-J. Kim, C. Kwon, R. Ramesh, and T. Venkatesan, Nature (London) **392**, 794 (1998).

[3] I. Galanakis, P. H. Dederichs, and N. Papanikolaou, Phys. Rev. B **66**, 174429 (2002).

[4] S. Picozzi, A. Continenza, and A. J. Freeman, Phys. Rev. B **66**, 094421 (2002).

[5] C. Felser, G. H. Fecher, and B. Balke, Angew. Chem., Int. Ed. **46**, 668 (2007).

[6] K. Inomata, S. Okamura, R. Goto, and N. Tezuka, Jpn. J. Appl. Phys., Part 2 **42**, L419 (2003).

[7] S. Kämmerer, A. Thomas, A. Hütten, and G. Reiss, Appl. Phys. Lett. **85**, 79 (2004).

[8] Y. Sakuraba, M. Hattori, M. Oogane, Y. Ando, H. Kato, A. Sakuma, T. Miyazaki, and H. Kubota, Appl. Phys. Lett. **88**, 192508 (2006).

[9] W. Wang, H. Sukegawa, R. Shan, and K. Inomata, Appl. Phys. Lett. **93**, 122506 (2008).

[10] S. Tsunegi, Y. Sakuraba, M. Oogane, K. Takanashi, and Y. Ando, Appl. Phys. Lett. **93**, 112506 (2008).

[11] N. Tezuka, N. Ikeda, F. Mitsuhashi, and S. Sugimoto, Appl. Phys. Lett. **94**, 162504 (2009).

[12] T. Taira, T. Ishikawa, N. Itabashi, K.-I. Matsuda, T. Uemura, and M. Yamamoto, J. Phys. D **42**, 084015 (2009).

[13] N. Tezuka, N. Ikeda, S. Sugimoto, and K. Inomata, Jpn. J. Appl. Phys., Part 2 **46**, L454 (2007).

[14] G. H. Fecher, H. C. Kandpal, S. Wurmehl, J. Morais, H.-J. Lin, H. J. Elmers, G. Schönhense, and C. Felser, J. Phys.: Condens. Matter **17**, 7237 (2005).

[15] K. Özdoğan, B. Aktaş, I. Galanakis, and E. Şaşıoğlu, J. Appl. Phys. **101**, 073910 (2007).

[16] L. Chioncel, Y. Sakuraba, E. Arrigoni, M. I. Katsnelson, M. Oogane, Y. Ando, T. Miyazaki, E. Burzo, and A. I. Lichtenstein, Phys. Rev. Lett. **100**, 086402 (2008).

[17] R. Shan, H. Sukegawa, W. H. Wang, M. Kodzuka, T. Furubayashi, T. Ohkubo, S. Mitani, K. Inomata, and K. Hono, Phys. Rev. Lett. **102**, 246601 (2009).

[18] Y. Sakuraba, K. Takanashi, Y. Kota, T. Kubota, M. Oogane, A. Sakuma, and Y. Ando, Phys. Rev. B **81**, 144422 (2010).

[19] G. H. Fecher, B. Balke, S. Ouardi, C. Felser, G. Schönhense, E. Ikenaga, J.-J. Kim, S. Ueda, and K. Kobayashi, J. Phys. D **40**, 1576 (2007).

[20] J. Schmalhorst, D. Ebke, A. Weddemann, A. Hütten, A. Thomas, G. Reiss, A. Turchanin, A. Gölzhäuser, B. Balke, and C. Felser, J. Appl. Phys. **104**, 043918 (2008).

[21] M. Kallmayer, P. Klaer, H. Schneider, E. Arbelo Jorge, C. Herbort, G. Jakob, M. Jourdan, and H. J. Elmers, Phys. Rev. B **80**, 020406(R) (2009).

[22] P. Klaer, M. Kallmayer, C. G. F. Blum, T. Graf, J. Barth, B. Balke, G. H. Fecher, C. Felser, and H. J. Elmers, Phys. Rev. B **80**, 144405 (2009).

[23] I. Galanakis, P. Mavropoulos, and P. H. Dederichs, J. Phys. D **39**, 765 (2006).

[24] H. C. Kandpal, G. H. Fecher, and C. Felser, J. Phys. D **40**, 1507 (2007).

[25] B. S. D. C. S. Varaprasad, A. Rajanikanth, Y. K. Takahashi, and K. Hono, Appl. Phys. Express **3**, 023002 (2010).

[26] H. C. Kandpal, V. Ksenofontov, M. Wojcik, R. Seshadri, and C. Felser, J. Phys. D **40**, 1587 (2007).

[27] J. Barth, G. H. Fecher, B. Balke, S. Ouardi, T. Graf, C. Felser, A. Shkabko, A. Weidenkaff, P. Klaer, H. J. Elmers, H. Yoshikawa, S. Ueda, and K. Kobayashi, Phys. Rev. B **81**, 064404 (2010).

[28] T. Graf, J. Barth, C. G. F. Blum, B. Balke, C. Felser, P. Klaer, and H.-J. Elmers, Phys. Rev. B (to be published).

[29] T. Graf, F. Casper, J. Winterlik, B. Balke, G. H. Fecher, and C. Felser, Z. Anorg. Allg. Chem. **635**, 976 (2009).

[30] N. D. Telling, P. S. Keatley, G. van der Laan, R. J. Hicken, E. Arenholz, Y. Sakuraba, M. Oogane, Y. Ando, and T. Miyazaki, Phys. Rev. B **74**, 224439 (2006).

[31] H. J. Elmers, G. H. Fecher, D. Valdaitsev, S. A. Nepijko, A. Gloskovskii, G. Jakob, G. Schönhense, S. Wurmehl, T. Block, C. Felser, P. C. Hsu, W. L. Tsai, and S. Cramm, Phys. Rev. B **67**, 104412 (2003).

[32] K. Miyamoto, A. Kimura, K. Iori, K. Sakamoto, T. Xie, T. Moko, S. Qiao, M. Taniguchi, and K. Tsuchiya, J. Phys.: Condens. Matter **16**, S5797 (2004).

[33] M. Sargolzaei, M. Richter, K. Koepernik, I. Opahle, H. Eschrig, and I. Chaplygin, Phys. Rev. B **74**, 224410 (2006).

[34] P. Blaha, K. Schwarz, G. K. H. Madsen, D. Kvasnicka, and J. Luitz, computer code WIEN2k, an augmented plane wave plus local orbitals program for calculating crystal properties, Vienna University of Technology, Vienna, 2001.

[35] J. Friedel, J. Phys. Radium **23**, 501 (1962).

[36] B. Balke, S. Wurmehl, G. H. Fecher, C. Felser, and J. Kübler, Sci. Technol. Adv. Mater. **9**, 014102 (2008).

[37] X.-Q. Chen, R. Podloucky, and P. Rogl, J. Appl. Phys. **100**, 113901 (2006).